

VEDA: 3D Molecular Generation via Variance-Exploding Diffusion with Annealing

Peining Zhang¹, Jinbo Bi¹, Minghu Song²

¹University of Connecticut, Storrs, Connecticut 06269, USA

²Institute of Health and Medicine, Hefei Comprehensive National Science Center, Hefei 230601, China
peining.zhang@uconn.edu, jinbo.bi@uconn.edu, minghu.song@ihm.ac.cn

Abstract

Diffusion models show promise for 3D molecular generation, but face a fundamental trade-off between sampling efficiency and conformational accuracy. While flow-based models are fast, they often produce geometrically inaccurate structures, as they have difficulty capturing the multimodal distributions of molecular conformations. In contrast, denoising diffusion models are more accurate but suffer from slow sampling, a limitation attributed to sub-optimal integration between diffusion dynamics and SE(3)-equivariant architectures. To address this, we propose **VEDA**, a unified SE(3)-equivariant framework that combines variance-exploding diffusion with annealing to efficiently generate conformationally accurate 3D molecular structures. Specifically, our key technical contributions include: (1) a VE schedule that enables noise injection functionally analogous to simulated annealing, improving 3D accuracy and reducing relaxation energy; (2) a novel preconditioning scheme that reconciles the coordinate-predicting nature of SE(3)-equivariant networks with a residual-based diffusion objective, and (3) a new arcsin-based scheduler that concentrates sampling in critical intervals of the logarithmic signal-to-noise ratio. On the QM9 and GEOM-DRUGS datasets, VEDA matches the sampling efficiency of flow-based models, achieving state-of-the-art valency stability and validity with only 100 sampling steps. More importantly, VEDA’s generated structures are remarkably stable, as measured by their relaxation energy (ΔE_{relax}) during GFN2-xTB optimization. The median energy change is only 1.72 kcal/mol, significantly lower than the 32.3 kcal/mol from its architectural baseline, SemlaFlow. Our framework demonstrates that principled integration of VE diffusion with SE(3)-equivariant architectures can achieve both high chemical accuracy and computational efficiency.

Code — <https://github.com/peiningzhang/VEDA>

Extended version — <https://arxiv.org/abs/2511.09568>

Introduction

Deep generative models are revolutionizing computational drug discovery. Breakthroughs like AlphaFold3 (Abramson et al. 2024) and RFDiffusion (Watson et al. 2023)

have shown the power of AI in protein structure prediction and design. Among them, diffusion models (Ho, Jain, and Abbeel 2020; Song et al. 2021) and their variants (Lipman et al. 2023), originally developed for computer vision, have emerged as a dominant tool for generating novel small molecules, a core task in drug discovery. Their ability to model continuous generative processes (i.e., transforming random noise into complex, structured data through a series of continuous steps) well aligns with the continuous coordinates of 3D molecular conformation. By representing molecules as 3D point clouds in Euclidean space and using equivariant architectures (e.g., equivariant graph neural networks (EGNNs) (Satorras, Hoogeboom, and Welling 2021) and E(3)-equivariant Transformers (Fuchs et al. 2020)), these models can generate geometrically realistic and chemically valid conformations (Hoogeboom et al. 2022).

In recent years, numerous diffusion models have been developed for 3D molecular generation or 3D molecular conformation generation. However, existing approaches have largely focused on refining their network architecture or by injecting domain-specific knowledge to guide the generation process—for instance, by developing novel equivariant transformers (Liao and Smidt 2023), shifting from direct 3D atom coordinates to internal coordinates like torsion angles (Jing et al. 2022), or explicitly modeling chemical bond interactions (Huang et al. 2023b)—while overlooking the principled design of the diffusion process itself (Zhang et al. 2025). A critical yet unaddressed question is how to redesign the learning objective to best match a unique characteristic of SE(3)-equivariant neural networks: their strong tendency to learn identity-like mappings, a bias stemming from their message-passing mechanism and strict geometric constraints. In diffusion models, this is often achieved through a technique called preconditioning, which provides a vital analytical framework to make the training objective more tractable (Karras et al. 2022). By aligning the objective with the model’s architectural inductive biases, this principled approach can significantly improve performance and training stability. Despite its potential, this promising direction remains largely overlooked in current molecular generative models.

To address this gap, we propose VEDA, a principled framework for 3D molecular diffusion where:

- To the best of our knowledge, VEDA is the first framework to apply the Variance-Exploding (VE) diffusion paradigm to the hybrid discrete-continuous domain of 3D molecules, unifying atomic types (discrete) and coordinates (continuous) within a single diffusion process that is functionally analogous to simulated annealing.
- We propose a theoretically grounded preconditioning scheme to correct the inductive bias of coordinate-predicting SE(3) equivariant networks. As a complementary innovation in diffusion dynamics, we introduce a noise schedule based on the arcsine function, which achieves a better balance between early-stage exploration and late-stage refinement in molecular generation.
- VEDA substantially reduces relaxation energy of generated molecules, by 90% compared to those generated by SemlaFlowa (Irwin et al. 2025), while achieving state-of-the-art performance on QM9 and GEOM-DRUGS, and matching the efficiency of strong flow-based models with significantly fewer sampling steps.

Related works

Diffusion-Based Generative Models Denoising Diffusion Probabilistic Models (DDPMs) (Ho, Jain, and Abbeel 2020) have become a leading class of generative models which learn to reverse a forward process that incrementally corrupts data with Gaussian noise. DDPMs are extended to continuous-time settings using score-based stochastic differential equations (SDEs) (Song et al. 2021), incorporating either variance-preserving or variance-exploding dynamics. Recent advances, particularly those utilizing Variance-Exploding (VE) SDEs with preconditioning techniques (Karras et al. 2022), have substantially enhanced generation quality and sampling efficiency. An alternative approach, Flow Matching (Lipman et al. 2023), directly learns the velocity field of the data distribution’s probability flow, offering a different yet highly competitive approach to generative modeling. Consistent with recent literature (Gao et al. 2024), we consider flow matching a specialized formulation within the broader diffusion framework.

Discrete Diffusion Models The principles of diffusion have also been extended to discrete data generation, drawing inspiration from masked language modeling (Devlin et al. 2019). These non-autoregressive methods are a natural fit for the unordered structure of molecules, enabling de novo generation without imposing artificial sequential or ordering assumptions. D3PM (Austin et al. 2021) established the theoretical foundations for discrete diffusion using continuous-time Markov chains. Subsequent developments of variants of Discrete Flow Matching (Campbell et al. 2024; Gat et al. 2024) have further advanced the field with improved sampling strategies and scalability.

De novo 3D Molecular Generation Modern 3D molecular generation heavily relies on E(3)-equivariant neural networks, from pioneering architectures like EGNN (Satorras, Hoogeboom, and Welling 2021) to subsequent transformer-

based models (Zhang, Chen, and Chu 2025). From a probabilistic modeling perspective, the field is dominated by a fundamental trade-off. Denoising diffusion-based methods like EDM (Hoogeboom et al. 2022) and GeoLDM (Xu et al. 2023) achieve high conformational accuracy but suffer from slow sampling. Conversely, flow-based models such as EquiFM (Song et al. 2023a), GeoBFN (Song et al. 2023c), and SemlaFlow (Irwin et al. 2025) are efficient but often struggle with geometric precision. Balancing high fidelity with computational efficiency remains a pressing challenge, with recent benchmarks underscoring the chemical inaccuracy of flow-based models (Nikitin et al. 2025).

Methodology

Preliminaries

We represent molecules as point clouds of chemical elements in 3D space, denoted by $\mathcal{M} = (\mathbf{x}, \mathbf{z})$, where $\mathbf{x} = (\mathbf{x}_1, \dots, \mathbf{x}_N) \in \mathbb{R}^{N \times 3}$ are the atomic coordinates of N atoms, and \mathbf{z} denotes non-geometric molecular attributes. To keep notation unified, we decompose $\mathbf{z} = (\mathbf{h}, \mathbf{b})$, where \mathbf{h} includes atom-level properties (e.g., atom types, charges) and \mathbf{b} denotes pairwise bond information.

In most graph-based models, a molecule is further represented by a graph $G = (V, E)$, where nodes V represent atoms and edges E represent either inferred or explicitly defined interactions between atoms. These interactions can be constructed based on distance thresholds or chemical bond annotations. Some models treat bond information as part of the output (explicit bond modeling), while others infer it post hoc based on generated atomic coordinates (implicit bond inference). This distinction influences the architecture and training strategy of generative models, as detailed later.

Model Architecture

To show our VEDA framework is both general and scalable, we apply it to two architectures at different levels of complexity. This dual implementation proves VEDA’s effectiveness across different modeling paradigms, covering both implicit and explicit bond generation.

VEDA-E: Implicit Bond Modeling The VEDA-E variant is built upon the EGNN architecture (Satorras, Hoogeboom, and Welling 2021) from EDM (Hoogeboom et al. 2022). In this setup, the model generates only node-centric features $\mathbf{h} = (\mathbf{h}_1, \dots, \mathbf{h}_N) \in \mathbb{R}^{N \times d_h}$, which include atom types and charges. Diffusion is performed by adding Gaussian noise to all continuous features. The chemical bond structure \mathbf{b} is not explicitly modeled during generation; instead, it is inferred post hoc based on interatomic distances and chemical valence rules, a standard practice in EDM-based molecule generation.

VEDA-S: Explicit Bond Modeling In contrast, VEDA-S adopts the Semla architecture from SemlaFlow (Irwin et al. 2025) to explicitly model bonds. This variant directly generates a complete molecular graph representation $\mathbf{z} = (\mathbf{h}, \mathbf{b})$,

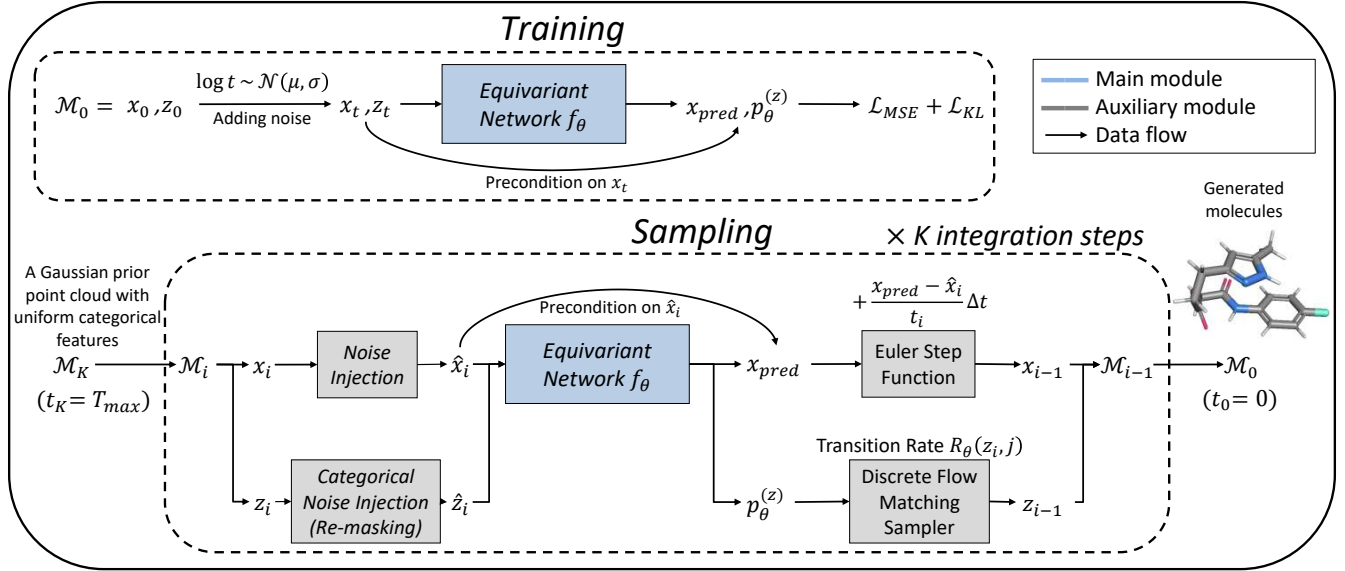


Figure 1: An overview of the VEDA framework, detailing its training and sampling processes. During **Training** (top), a clean molecule \mathcal{M}_0 is perturbed via Gaussian noise for coordinates (\mathbf{x}_t) and categorical corruption for features (\mathbf{z}_t), defined by Eq. 1 and Eq. 3. The equivariant network f_θ is then trained to predict the original molecule by minimizing the combined Mean Squared Error (MSE) and Cross-Entropy (CE) loss in Eq. 12. During **Sampling** (bottom), the process starts from a pure noise distribution (a Gaussian point cloud with uniform categorical features) and iteratively refines the sample over K steps. Each integration step i involves: (1) a noise injection from $(\mathbf{x}_i, \mathbf{z}_i)$ to $(\hat{\mathbf{x}}_i, \hat{\mathbf{z}}_i)$; (2) the network f_θ is applied to both coordinates and features, with preconditioning affecting only the coordinate predictions; it outputs x_{pred} and the category probabilities $p_\theta^{(z)}$ (Eq. 6); and (3) an update combining a continuous Euler step and a Discrete Flow Matching sampler to obtain \mathcal{M}_{i-1} , formally given in Eq. 13 and Eq. 14. In the diagram, blue boxes represent the main network module, gray boxes are auxiliary operations, and arrows indicate the data flow.

where \mathbf{h} represents node features and $\mathbf{b} \in \mathbb{R}^{N \times N \times d_b}$ denotes the bond types between atoms. This approach is compatible with discrete data types by using a mask-based diffusion process and a classification objective. A diagram illustrating the main concept of VEDA-S is provided in Figure 1.

Diffusion Dynamics

Our generative model is based on Score Diffusion (Song et al. 2021). It includes a forward diffusion process gradually perturbing the clean data into noise, and a learned denoising process that recover the noise into data. The denoising process is governed by the denoiser D_θ , which takes as input the noisy sample \mathbf{x}_t and the noise level t . We define \mathbf{x}_0 as the clean data point (e.g., molecular coordinates) and \mathbf{x}_∞ as the fully noised sample.

Forward Process We corrupt the continuous coordinates \mathbf{x} by adding Gaussian noise:

$$\mathbf{x}_t = \mathbf{x}_0 + t\epsilon, \quad \epsilon \sim \mathcal{N}(0, I), \quad (1)$$

The noise level t is sampled from a log-normal distribution: $\log(t) \sim \mathcal{N}(\ln \sqrt{T_{\min} T_{\max}}, [\frac{1}{8} \ln(T_{\max}/T_{\min})]^2)$, so $t \in [T_{\min}, T_{\max}]$ in most case.

For discrete features \mathbf{z} , we consider two variants.

In **VEDA-E**, Gaussian noise is applied:

$$\mathbf{z}_t = \mathbf{z}_0 + t\eta, \quad \eta \sim \mathcal{N}(0, I). \quad (2)$$

In **VEDA-S**, we use time-dependent categorical corruption:

$$\mathbf{z}_t \sim \text{Cat} \left[(1 - m(t)) \delta(\mathbf{z}_t = \mathbf{z}_0) + \frac{m(t)}{S} \right], \quad (3)$$

where S is the number of categories, and the masking rate function $m(t) = (\ln t - \ln T_{\min}) / (\ln T_{\max} - \ln T_{\min})$ aligns the discrete corruption schedule with the continuous noise schedule, reaching uniform distribution at $t = T_{\max}$.

Our approach uses this principled VE scheduler during training. This variance-exploding (VE) formulation is particularly suitable for modeling continuous data such as 3D molecular structures, as it enables flexible noise schedules and accurate noise level control in log-space, injecting a massive amount of noise to reach lower energy. We believe infinite separation at $t \rightarrow \infty$ between atoms is an ideal noisy state for molecule generation, superior to a standard Gaussian prior, as it corresponds to no chemical interactions between atoms.

Preconditioning the Denoiser In 3D molecular generation with diffusion models, directly predicting coordinates (x -prediction) is the prevailing approach, as equivariant network architectures like GNNs are not well-suited for predicting noise or velocity (Irwin et al. 2025). We adopt the preconditioning framework from Karras et al. (2022), where the denoiser D_θ is defined as a combination of the input \mathbf{x}_t

and a neural network output F_θ :

$$D_\theta(\mathbf{x}_t; t) = c_{\text{skip}}\mathbf{x}_t + c_{\text{out}}[F_\theta(c_{\text{in}}\mathbf{x}_t; c_{\text{noise}})] \quad (4)$$

$$F_{\text{target}} = \frac{1}{c_{\text{out}}}(\mathbf{x}_0 - c_{\text{skip}}(\mathbf{x}_0 + t\epsilon)) \quad (5)$$

Optimizing the preconditioning framework with a coordinate-space MSE loss requires the network (F_θ) to output residuals that are uncorrelated with the input. However, our backbone (GNN or Graph Transformer) outputs coordinates via a residual connection design (He et al. 2016), which causes F_θ to produce outputs highly correlated with \mathbf{x}_t , conflicting with the residual learning objective.

To address this mismatch, we subtract a scaled identity component from the network output. Instead of forcing the network to suppress its inherent bias through the loss function, we explicitly subtract the undesired identity component from its output. Our modified denoiser is:

$$D_\theta(\mathbf{x}_t; t) = c_{\text{skip}}\mathbf{x}_t + c_{\text{out}}(F_\theta(c_{\text{in}}\mathbf{x}_t; c_{\text{noise}}) - \alpha_t c_{\text{in}}\mathbf{x}_t) \quad (6)$$

The coefficient α_t is our main contribution in this section. It serves as the optimal linear predictor of the ground-truth noise $\frac{\sigma_d\epsilon}{\sqrt{\sigma_d^2 + t^2}}$ from F_{target} , where σ_d is the standard deviation of the data distribution (Karras et al. 2022). This corresponds to the Linear Minimum Mean Squared Error (LMMSE) solution, which yields the following closed-form coefficient:

$$\alpha_t = \arg \min_{\alpha} \mathbb{E}[\|\frac{\sigma_d\epsilon}{\sqrt{\sigma_d^2 + t^2}} - \alpha c_{\text{in}}\mathbf{x}_t\|^2] \quad (7)$$

$$= \arg \min_{\alpha} \mathbb{E}[\|\sigma_d\epsilon - \alpha t\mathbf{x}_t\|^2] \quad (8)$$

$$= \frac{\text{Cov}(\sigma_d\epsilon, \mathbf{x}_t)}{\text{Var}(\mathbf{x}_t)} = \frac{\sigma_d t}{\sigma_d^2 + t^2} \quad (9)$$

Using this optimal α_t reduces the residual correlation with the input and better aligns the training objective with the network’s inductive bias, i.e., its preference for modeling absolute coordinates. (See Appendix I for derivation.) We use the standard definitions of c_{skip} , c_{out} , c_{in} , c_{noise} , and λ_σ from Karras et al. (2022).

Training Objectives

For VEDA-E, we apply a mean squared error (MSE) loss to both continuous coordinates and categorical features:

$$\mathcal{L}_{\text{MSE}} = \mathbb{E}_{\mathbf{x}_0, \mathbf{z}_0, \epsilon, t} [\|D_\theta(\mathbf{x}_t, \mathbf{z}_t; t) - (\mathbf{x}_0, \mathbf{z}_0)\|^2], \quad (10)$$

where $(\mathbf{x}_0, \mathbf{z}_0)$ represents the concatenated true coordinates and categorical features. Following the implementation of EDM (Hoogeboom et al. 2022), VEDA-E treats categorical features \mathbf{z}_0 as continuous during denoising and applies MSE loss, despite their inherently discrete nature..

For VEDA-S, the model predicts the original discrete features \mathbf{z}_0 via a categorical distribution $\hat{p}_\theta(\mathbf{z}_0 | \tilde{\mathbf{z}}_t, t)$. This is optimized using a KL divergence loss:

$$\mathcal{L}_{\text{KL}} = \mathbb{E}_{\mathbf{z}_0, \tilde{\mathbf{z}}_t, t} [\text{KL}(\delta(\mathbf{z}_0) \| \hat{p}_\theta(\mathbf{z}_0 | \tilde{\mathbf{z}}_t, t))]. \quad (11)$$

The overall loss combines continuous and discrete terms:

$$\mathcal{L}_{\text{VEDA-S}} = \lambda_{\text{cont}} \mathcal{L}_{\text{MSE}} + \lambda_{\text{disc}} \mathcal{L}_{\text{KL}} \quad (12)$$

where λ_{cont} and λ_{disc} balance the two objectives.

Sampling

We adopt the standard denoising framework where the generative process iteratively refines noisy inputs into data samples, following a predefined SDE formulation (Karras et al. 2022). Conceptually, this process is analogous to *simulated annealing*. The noise level t acts as a temperature parameter that is gradually lowered, enabling broad exploration of the energy landscape at high noise and convergence to low-energy, stable conformations as noise decreases. Our model operates under the x -prediction parameterization to directly estimate the clean sample from its noisy counterpart. During sampling, VEDA-E applies continuous noise injection to all features, while VEDA-S uses continuous noise injection for coordinates and discrete token refinement for categorical features. We now describe three interlocking sampling components: (1) continuous denoising with amplified noise injection, (2) discrete masked-token refinement, and (3) the proposed arcsin noise scheduler.

Stochastic Annealing for Continuous Coordinates Our sampling process employs an amplified noise injection strategy. This approach is governed by a hyperparameter, $\gamma > 0$, which controls the degree of noise amplification. This process is equivalent in expectation to Gaussian smoothing on the molecular potential energy surface with a Gaussian kernel bandwidth of $\sqrt{\gamma^2 + 2\gamma} \cdot t_i$ (See Appendix J for deviation). This pronounced smoothing suppresses local minima and surface roughness, making it easier for the sample trajectory to find the global low-energy basin and thereby improving the final energy metric (Miao, Feher, and McCammon 2015).

Sampling proceeds in two substeps for each iteration i :

1. **Perturbation:** We first set the value of $\hat{t}_i = (1 + \gamma)t_i$ inject amplified noise into the current sample \mathbf{x}_i to reach an intermediate state $\hat{\mathbf{x}}_i = \mathbf{x}_i + \sqrt{\hat{t}_i^2 - t_i^2} \cdot \epsilon$, where $\epsilon \sim \mathcal{N}(0, I)$. The noise added is substantially greater than in standard DDPM (Ho, Jain, and Abbeel 2020) or Flow-Matching (Lipman et al. 2023) schedules.
2. **Denoising & Update:** The denoiser $D_\theta(\hat{\mathbf{x}}_i; \hat{t}_i)$ predicts the clean structure, from which we extrapolate the next sample \mathbf{x}_{i+1} via a Euler step:

$$\mathbf{x}_{i+1} = \hat{\mathbf{x}}_i + \frac{t_{i+1} - \hat{t}_i}{\hat{t}_i}(\hat{\mathbf{x}}_i - D_\theta(\hat{\mathbf{x}}_i; \hat{t}_i)). \quad (13)$$

In VEDA-E, this two-step procedure is applied uniformly to both coordinates and categorical features. In VEDA-S, only the coordinates undergo amplified noise injection, while categorical features are handled separately via discrete token refinement.

Masked Token Refinement for Discrete Variables For discrete features in VEDA-S, we use masked token refinement process. This process is governed by the time-dependent mask rate function $m(t)$, which is designed to align the discrete corruption with the continuous noise schedule. Specifically, when injecting noise from noise level

t_1 to t_2 , each token is randomly re-masked with probability $\frac{m(t_2)-m(t_1)}{1-m(t_1)}$. Additionally, we found that a simple uniform random re-masking strategy consistently outperformed more complex confidence-based strategies proposed in prior work (Nie et al. 2025). We included our comparison with the strategies of low prediction confidence (Chang et al. 2022) or small probability margins (Kim et al. 2025) in Appendix B.

For discrete sampling, our approach is a step-wise masked sampling algorithm based on Continuous-Time Markov Chains (CTMC) within the Discrete Flow Matching framework. We implement and compare two complementary sampling strategies based on this foundation.

The full transition rate combines base interpolation dynamics with detailed balance corrections:

$$R_\theta(z_t, j) = \omega(t) \cdot p_\theta(z_0 = j | z_t) + \eta_t \cdot p_\theta(z_0 = z_t | z_t) \quad (14)$$

where $\omega(t) = \frac{\eta_t S(1-m(t)) + \eta_t m(t) + m'(t)}{m(t)}$ is the time-dependent scaling factor, and η_t is based on the categorical noise hyperparameter η . To determine the optimal configuration, we performed a comprehensive grid search. The results confirmed that the variable setting from Campbell et al. (2024), where $\eta_t = \frac{\eta}{m'(t)}$, achieves the best and most robust performance, outperforming both the fixed setting ($\eta_t = \eta$) and the simplified DFM formulation from Gat et al. (2024). The transition rates are thus derived to optimally combine the model’s confidence in clean data predictions with the stability of maintaining current token assignments (see Appendices G, H for derivations and C for grid search details).

Proposed Noise Scheduler We propose an **arcsin-based noise scheduler** that further improves the sampling process. Through empirical analysis, we observe that sampling steps corresponding to near-zero log signal-to-noise ratio (log-SNR), i.e. $\log(\text{signal variance}/\text{noise variance})$ are especially critical for final molecular structure formation. It aligns well with the distribution of $t \sim \text{LogNormal}(\ln \sqrt{T_{\min} T_{\max}}, [\frac{1}{8} \ln(T_{\max}/T_{\min})]^2)$ used during training. To leverage this observation, let $u = i/N$ is the normalized step index for a total of N steps. We design an arcsin-shaped scheduler parameterized by a tunable scalar ρ . Our scheduler is defined as:

$$w(u) = (1 - \rho)u + \rho \frac{2}{\pi} \arcsin(\sqrt{u}) \quad (15)$$

$$t^{(i)} = T_{\min} \left(\frac{T_{\max}}{T_{\min}} \right)^{w(u)} \quad (16)$$

Where $\rho \in [0, \frac{\pi}{\pi-2}]$ modulates the concentration around $\log\text{-SNR} \approx 0$. When $\rho = 0$, the scheduler reduces to a log-uniform schedule commonly used in prior work; as ρ increases, more steps cluster in the mid-range. This targeted allocation of sampling steps improves structural fidelity and overall sample quality, especially in chemically sensitive configurations. As shown in Figure 2, the arcsin scheduler ($\rho=2$) closely matches the log-normal training distribution, further supporting its design rationale.

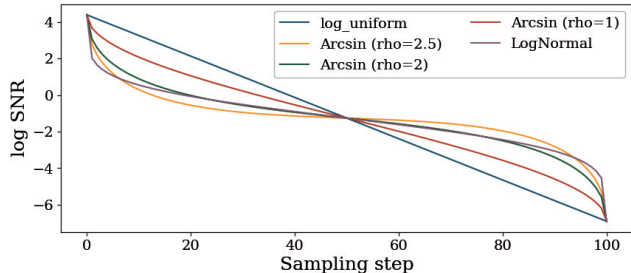


Figure 2: The arcsin sampling scheduler is proposed to focus on the middle part of sampling where $\log(\text{SNR})$ is close to 0

Methods	NFE ↓	Atom Sta(%)↑	Mol Sta(%)↑	Valid (%)↑	Valid & Unique(%)↑
EDM	1000	98.7	82	91.9	90.9
GeoLDM	1000	98.9	89.4	93.8	92.6
UniGEM	1000	99.0	89.8	95	93.2
EquiFM	210	98.9	88.3	94.7	93.5
GeoBFN	2000	99.3	93.3	96.9	92.4
GOAT	90	99.2	-	92.9	92.0
VEDA-E	50	99.4	93.7	98.1	97.9
VEDA-E	30	99.2	91.5	97.0	96.8
MiDi	500	97.5	97.9	95.5	-
FlowMol2	100	99.9	99.6	99.5	-
EQGAT-diff	500	99.9	98.7	99.0	98.8
SemlaFlow	100	99.9	99.7	99.4	98.7
VEDA-S	100	100.0	99.9	99.6	98.9
VEDA-S	50	100.0	99.7	99.4	98.4
VEDA-S	30	99.9	99.5	99.5	98.9

Table 1: **Results on QM9.** *Top*: bond-implicit methods (bonds inferred from coordinates); *Bottom*: bond-explicit methods (bonds generated directly). NFE = number of function evaluations (sampling steps). Best in each group in **bold**.

Experiments

Experimental Setup

Model Variants To evaluate our VE-diffusion paradigm, we implement two variants based on distinct backbones. **VEDA-E** is built upon the EDM framework (Hooeboom et al. 2022), using an EGNN backbone and performing implicit bond modeling. In contrast, **VEDA-S** derives from the SemlaFlow framework (Irwin et al. 2025), adopting a Semla backbone for explicit bond modeling.

Datasets and Metrics We evaluate our models on QM9 (Ramakrishnan et al. 2014) and GEOM-DRUGS (Axelrod and Gomez 2022) using distinct protocols. For QM9, we report standard metrics for chemical correctness: Atom Stability (Atom Sta.), Molecule Stability (Mol Sta.), Validity, and Unique percentage. For the more complex GEOM-DRUGS dataset, our main analysis followed the protocol proposed by Nikitin et al. (2025), which prioritizes physical realism, reporting the fixed version of molecular stability and validity alongside key metrics from GFN2-xTB geometry optimization, such as relaxation energy (ΔE_{relax}), post-optimization RMSD, and the structural difference after optimization. A supplementary analysis using the MMFF94 (Halgren 1996) force field to assess conformational energy and strain is detailed in the Appendix B.

Model	NFE	Time (s)	MS \uparrow	V&C \uparrow	Bond Length \downarrow ($\times 10^{-2}$)	Bond Angles \downarrow	Tor. \downarrow	Median ΔE_{relax} \downarrow	Mean ΔE_{relax} \downarrow	Median RMSD \downarrow	Mean RMSD \downarrow
EQGAT	500	3468	0.899	0.834	1.00	1.15	8.58	6.40	11.1	0.915	0.975
JODO	500	673	0.963	0.879	0.77	0.83	6.01	4.74	7.04	-	-
Megalodon-quick	500	-	0.944	0.900	0.66	0.71	5.58	3.19	5.76	-	-
FlowMol2	100	126.3	0.944	0.746	1.30	1.62	15.0	17.9	24.3	0.992	1.038
SemlaFlow	100	150.3	0.969	0.920	3.10	2.06	6.05	32.3	91.0	0.273	0.358
Megalodon-flow	100	-	0.987	0.948	2.30	1.62	5.58	20.9	46.9	-	-
VEDA-S	100	164.8	0.995	0.988	0.69	0.41	2.71	1.72	2.93	0.096	0.197
VEDA-S	50	84.1	0.968	0.966	0.86	0.60	5.10	2.99	8.38	0.236	0.355

Table 2: **Performance comparison on the GEOM-DRUGS dataset.** Our model, VEDA-S (bottom), is compared against denoising-based (top) and flow-based (middle) methods. **Bold** values indicate the best result. Metrics include Molecular Stability (MS), Validity & Connectivity (V&C), and Mean Absolute Error (MAE) for bond lengths, angles, and torsions. All metrics are lower-is-better except for MS and V&C. Time (s) reports the average wall-clock time for generating one molecule. NFE is the Number of Function Evaluations. RMSD values for some models are missing as they were not in the original benchmark. For each model, 5000 molecules were evaluated, the full results with confidence intervals and sampling at other steps are included in Appendix B.

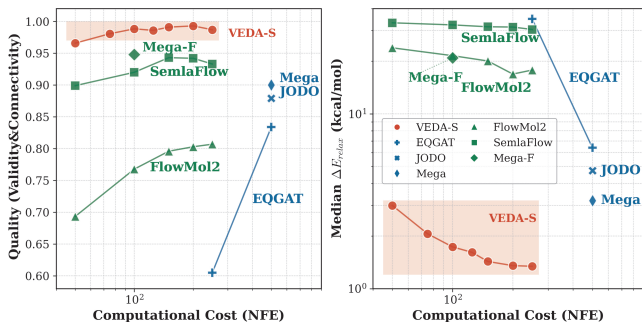


Figure 3: Trade-off between Generation Quality and Computational Cost. The figure compares our model, VEDA-S (red), against flow-based (green) and denoising-based (blue) models. The horizontal axis represents the computational cost, measured by the Number of Function Evaluations (NFE). (Left) Quality measured by molecule Validity and Connectivity, where higher values are better. (Right) Quality measured by the median energy difference (ΔE_{relax}), where lower values are better.

Baselines We compare VEDA against leading 3D molecular generative models, grouped by bond treatment. For methods that do not explicitly generate bond structures, we consider EDM (Hooeboom et al. 2022), GeoLDM (Xu et al. 2023), EquiFM (Song et al. 2023b), GeoBFN (Song et al. 2023c), UniGEM (Feng et al. 2024) and GOAT (Hong, Lin, and Tan 2024), all of which use equivariant architectures. For methods with explicit bond modeling, we compare to SemlaFlow (Irwin et al. 2025), FlowMol2 (Dunn and Koes 2024), and JODO (Huang et al. 2023a), EQGAT-diff (Le et al. 2024) and Megalodon (Reidenbach et al. 2025).

Main Results

Results on QM9 As shown in Table 1, our model VEDA achieves state-of-the-art performance on the QM9 dataset. In the bond-implicit setting, VEDA-E achieves the highest valid and unique rate (97.9%) with only 50 NFE, significantly outperforming methods like EDM (90.9% at 1000 NFE) and GeoLDM (92.6% at 1000 NFE). In the bond-explicit setting, VEDA-S achieves nearly perfect atom stability and molecular stability, and a valid and unique score

of 98.9% at just 100 NFE. Even at 30 NFE, it remains competitive with most baselines, highlighting its efficiency.

Results on GEOM-DRUGS We evaluate our model on the GEOM-DRUGS dataset using the protocol from Nikitin et al. (2025), with detailed metrics provided in Table 2. As the results show, our VEDA-S model achieves a new state-of-the-art performance across nearly all metrics. Notably, this is accomplished in just 100 function evaluations (NFE), significantly outperforming computationally expensive 500-step models like Megalodon, and surpassing previous flow-based approaches by a large margin in geometric accuracy.

This superior performance is not just in final quality but also in the trade-off between sampling efficiency and generation quality, as shown in Figure 3. The figure plots generation quality as a function of NFE. Quality is assessed by both validity and geometric stability, measured via median relaxation energy. The results are striking: VEDA-S (in red) consistently occupies the optimal region in both plots. It achieves the high efficiency of flow-based models (green) while delivering a geometric accuracy (lower ΔE_{relax}) that is an order of magnitude better than all competitors.

To further validate this comparison, we also tested noise-injected sampling for SemlaFlow (See Appendix B), but observed no significant gains. However, this modification did not lead to significant improvements. This finding suggests that VEDA’s superior performance arises not merely from the presence of noise, but from its systematic framework design. Even on saturated metrics like molecular stability, our model pushes the scores closer to 100%. Furthermore, even with just 50 steps, VEDA-S remains highly competitive, demonstrating its excellent trade-off between sampling efficiency and generation quality.

Ablation Studies

Component Ablation Table 3 presents an ablation study on the GEOM-DRUGS dataset. We start from the full VEDA model and progressively remove key components to assess their impact. Disabling preconditioning refers to setting α_t

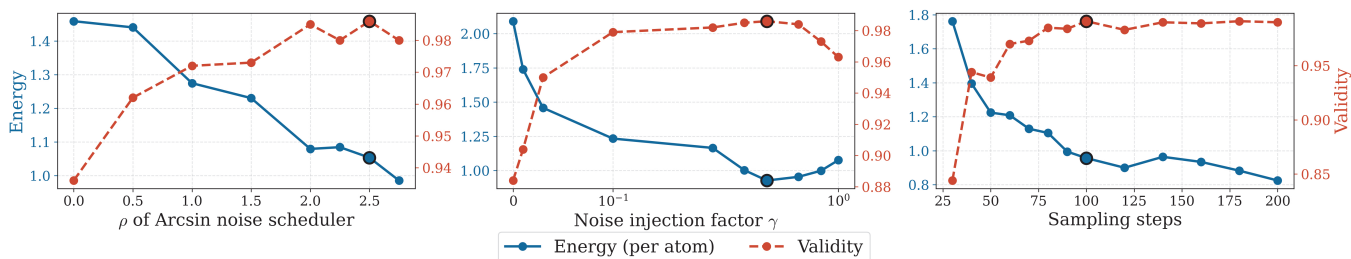


Figure 4: Ablation study of key hyperparameters on GEOM-DRUGS: We report MMFF94 energy and validity when varying (left) arcsin noise factor ρ , (middle) noise injection level γ , and (right) sampling steps. Black circles indicate selected values ($\rho=2.5$, $\gamma=0.4$, 100 steps).

to be 0. It results in a small drop in validity and modest increases in RMSD and relaxation error, showing the stabilizing effect of preconditioning. Removing the noise injection leads to a substantial drop in all metrics, highlighting its importance in guiding the denoising process. Introducing the optimal transport (OT) alignment mechanism, as used in SemlaFlow (Irwin et al. 2025), increases validity but significantly worsens energy and RMSD. We attribute this to OT alignment violating the independence assumption between noise and original molecular coordinates, which causes the denoising direction to become overly correlated with the aligned noise. This results in a collapse of coordinate variance during sampling and degrades overall sample quality. These results show that each module in VEDA provides complementary improvements to accuracy and validity.

Variant	OT	Noise	Pre	V&C \uparrow	M.S. \uparrow	E. \downarrow	R. \downarrow
VEDA (Full)	\times	\checkmark	\checkmark	98.8	99.5	1.72	0.096
– Pre	\times	\checkmark	\times	97.9	98.5	2.14	0.153
– Noise	\times	\times	\checkmark	95.9	97.6	6.29	0.382
– Noise & Pre	\times	\times	\times	93.8	92.9	10.1	0.409
+ OT Align	\checkmark	\times	\times	91.7	96.0	23.5	0.557
SemlaFlow	\checkmark	\times	\times	92.0	96.9	32.3	0.273

Table 3: **Ablation study on GEOM-DRUGS.** Each variant enables (\checkmark) or disables (\times) key components of VEDA: OT alignment (OT), noise injection (Noise), and preconditioning (Pre). V&C \uparrow and M.S. \uparrow are reported as percentage-based metrics. The last two rows share the same component configuration and differ only in their time parameterization (VE vs. FM).

Hyperparameter Sensitivity We performed a sensitivity analysis to support our final hyperparameter choices, as shown in Figure 4. For the arcsin scheduler factor, ρ , the model performs robustly across $\rho \in [2.0, 2.75]$, approaching the theoretical limit where the scheduler function remains monotonic. For the noise injection level γ follows the expected annealing behavior, where an intermediate value achieves the best trade-off. Finally, validity saturates around 100 sampling steps, offering an efficient trade-off between quality and cost.

Discussion

Our findings regarding optimal transport alignment, used in prior works like SemlaFlow (Irwin et al. 2025), reveals a critical design principle: training strategies must not only improve the loss but also consider their impact on downstream sampling. Our ablation study shows that seemingly

beneficial optimizations can violate core statistical assumptions—like noise-data independence—that are crucial for generating diverse and valid molecules.

While two-step (e.g., 2D or SMILES-to-3D) generation pipeline are often considered simpler and more scalable, we argue that native 3D generative capability is essential for designing functional molecules in constrained environments like protein pockets. This necessity is underscored by recent benchmarks showing that current target-aware diffusion models frequently produce invalid geometric structures, despite their high docking scores (Baillif et al. 2024). Therefore, enhancing the foundational 3D generative model, as we have focused on in this work, is critical for future success in structure-based design.

Conclusions

In this work, we introduced **VEDA**, a novel equivariant generative model for 3D molecular structures that unifies continuous and discrete generative processes within a single framework. Through comprehensive experiments on QM9 and GEOM-DRUGS, we show that VEDA not only surpasses strong baselines like GeoBFN and SemlaFlow in structural validity and stability metrics, but also delivers efficient generation thanks to its unified diffusion framework. Ablations studies validate that both the amplified VE noise schedule and the discrete sampling mechanism are critical to VEDA’s performance.

The success of VEDA in unconditional generation establishes a robust foundation, opening a clear and immediate path toward property-guided molecular design. A natural extension is to condition the generative process on target chemical properties such as binding affinity or solubility, leveraging VEDA’s unified framework to guide generation toward desired molecular profiles. Beyond conditional generation, we identify a fundamental limitation shared across current diffusion models: reliance on implicit velocity prediction through score matching. Future equivariant architectures should be designed to explicitly output the time-dependent vector field $v_\theta(\mathbf{x}, t)$. This would align training objectives with advanced samplers like Consistency Flow Matching (Lu and Song 2025) and MeanFlow (Geng et al. 2025), further improving sampling efficiency and unlocking one- or few-step integration.

The power of VEDA lies in its core approach: it uses VE diffusion to smooth the geometric landscape with controlled

noise, while seamlessly integrating discrete atomic features. This principled fusion of dynamics and geometry offers an effective blueprint for the future of molecular design.

References

- Abramson, J.; Adler, J.; Dunger, J.; Evans, R.; Green, T.; Pritzel, A.; Ronneberger, O.; Willmore, L.; Ballard, A. J.; Bambrick, J.; et al. 2024. Accurate structure prediction of biomolecular interactions with AlphaFold 3. *Nature*, 1–3.
- Austin, J.; Johnson, D. D.; Ho, J.; Tarlow, D.; and Van Den Berg, R. 2021. Structured denoising diffusion models in discrete state-spaces. *Advances in neural information processing systems*, 34: 17981–17993.
- Axelrod, S.; and Gomez, R., Bombarelli. 2022. GEOM, energy-annotated molecular conformations for property prediction and molecular generation. *Scientific Data*, 9(1): 185.
- Baillif, B.; Cole, J.; McCabe, P.; and Bender, A. 2024. Benchmarking structure-based three-dimensional molecular generative models using GenBench3D: ligand conformation quality matters. *arXiv preprint arXiv:2407.04424*.
- Campbell, A.; Yim, J.; Barzilay, R.; Rainforth, T.; and Jaakkola, T. 2024. Generative Flows on Discrete State-Spaces: Enabling Multimodal Flows with Applications to Protein Co-Design. In *International Conference on Machine Learning*, 5453–5512. PMLR.
- Chang, H.; Zhang, H.; Jiang, L.; Liu, C.; and Freeman, W. T. 2022. Maskgit: Masked generative image transformer. In *Proceedings of the IEEE/CVF conference on computer vision and pattern recognition*, 11315–11325.
- Devlin, J.; Chang, M.-W.; Lee, K.; and Toutanova, K. 2019. Bert: Pre-training of deep bidirectional transformers for language understanding. In *Proceedings of the 2019 conference of the North American chapter of the association for computational linguistics: human language technologies, volume 1 (long and short papers)*, 4171–4186.
- Dunn, I.; and Koes, D. R. 2024. Exploring Discrete Flow Matching for 3D De Novo Molecule Generation. *ArXiv*, arXiv:2411.
- Feng, S.; Ni, Y.; Lu, Y.; Ma, Z.-M.; Ma, W.-Y.; and Lan, Y. 2024. UniGEM: A Unified Approach to Generation and Property Prediction for Molecules. *arXiv preprint arXiv:2410.10516*.
- Fuchs, F.; Worrall, D.; Fischer, V.; and Welling, M. 2020. Se (3)-transformers: 3d roto-translation equivariant attention networks. *Advances in neural information processing systems*, 33: 1970–1981.
- Gao, R.; Hoogeboom, E.; Heek, J.; Bortoli, V.; Murphy, K. P.; and Salimans, T. 2024. Diffusion meets flow matching: Two sides of the same coin. *The Internet*.
- Gat, I.; Remez, T.; Shaul, N.; Kreuk, F.; Chen, R. T.; Synnaeve, G.; Adi, Y.; and Lipman, Y. 2024. Discrete flow matching. *Advances in Neural Information Processing Systems*, 37: 133345–133385.
- Geng, Z.; Deng, M.; Bai, X.; Kolter, J. Z.; and He, K. 2025. Mean flows for one-step generative modeling. *arXiv preprint arXiv:2505.13447*.
- Halgren, T. A. 1996. Merck molecular force field. I. Basis, form, scope, parameterization, and performance of MMFF94. *Journal of computational chemistry*, 17(5-6): 490–519.
- He, K.; Zhang, X.; Ren, S.; and Sun, J. 2016. Deep residual learning for image recognition. In *Proceedings of the IEEE conference on computer vision and pattern recognition*, 770–778.
- Ho, J.; Jain, A.; and Abbeel, P. 2020. Denoising diffusion probabilistic models. *Advances in neural information processing systems*, 33: 6840–6851.
- Hong, H.; Lin, W.; and Tan, K. C. 2024. Accelerating 3D Molecule Generation via Jointly Geometric Optimal Transport. In *The Thirteenth International Conference on Learning Representations*.
- Hoogeboom, E.; Satorras, V. G.; Vignac, C.; and Welling, M. 2022. Equivariant diffusion for molecule generation in 3d. In *International conference on machine learning*, 8867–8887. PMLR.
- Huang, H.; Sun, L.; Du, B.; and Lv, W. 2023a. Learning Joint 2D & 3D Diffusion Models for Complete Molecule Generation. *CoRR*.
- Huang, L.; Zhang, H.; Xu, T.; and Wong, K.-C. 2023b. Mdm: Molecular diffusion model for 3d molecule generation. In *Proceedings of the AAAI Conference on Artificial Intelligence*, volume 37, 5105–5112.
- Irwin, R.; Tibo, A.; Janet, J. P.; and Olsson, S. 2025. SemlaFlow – Efficient 3D Molecular Generation with Latent Attention and Equivariant Flow Matching. In *The 28th International Conference on Artificial Intelligence and Statistics*.
- Jing, B.; Corso, G.; Chang, J.; Barzilay, R.; and Jaakkola, T. 2022. Torsional diffusion for molecular conformer generation. *Advances in neural information processing systems*, 35: 24240–24253.
- Karras, T.; Aittala, M.; Aila, T.; and Laine, S. 2022. Elucidating the design space of diffusion-based generative models. *Advances in neural information processing systems*, 35: 26565–26577.
- Kim, J.; Shah, K.; Kontonis, V.; Kakade, S. M.; and Chen, S. 2025. Train for the Worst, Plan for the Best: Understanding Token Ordering in Masked Diffusions. In *Forty-second International Conference on Machine Learning*.
- Le, T.; Cremer, J.; Noe, F.; Clevert, D.-A.; and Schütt, K. T. 2024. Navigating the Design Space of Equivariant Diffusion-Based Generative Models for De Novo 3D Molecule Generation. In *The Twelfth International Conference on Learning Representations*.
- Liao, Y.-L.; and Smidt, T. 2023. Equiformer: Equivariant Graph Attention Transformer for 3D Atomistic Graphs. In *The Eleventh International Conference on Learning Representations*.
- Lipman, Y.; Chen, R. T.; Ben-Hamu, H.; Nickel, M.; and Le, M. 2023. Flow Matching for Generative Modeling. In *11th International Conference on Learning Representations, ICLR 2023*.

- Lu, C.; and Song, Y. 2025. Simplifying, Stabilizing and Scaling Continuous-time Consistency Models. In *The Thirteenth International Conference on Learning Representations*.
- Miao, Y.; Feher, V. A.; and McCammon, J. A. 2015. Gaussian accelerated molecular dynamics: unconstrained enhanced sampling and free energy calculation. *Journal of chemical theory and computation*, 11(8): 3584–3595.
- Nie, S.; Zhu, F.; You, Z.; Zhang, X.; Ou, J.; Hu, J.; ZHOU, J.; Lin, Y.; Wen, J.-R.; and Li, C. 2025. Large Language Diffusion Models. In *ICLR 2025 Workshop on Deep Generative Model in Machine Learning: Theory, Principle and Efficacy*.
- Nikitin, F.; Dunn, I.; Koes, D. R.; and Isayev, O. 2025. GEOM-Drugs Revisited: Toward More Chemically Accurate Benchmarks for 3D Molecule Generation. *arXiv preprint arXiv:2505.00169*.
- Ramakrishnan, R.; Dral, P. O.; Rupp, M.; and Von Lilienfeld, O. A. 2014. Quantum chemistry structures and properties of 134 kilo molecules. *Scientific data*, 1(1): 1–7.
- Reidenbach, D.; Nikitin, F.; Isayev, O.; and Paliwal, S. 2025. Applications of Modular Co-Design for De Novo 3D Molecule Generation. *arXiv preprint arXiv:2505.18392*.
- Satorras, V. G.; Hoogeboom, E.; and Welling, M. 2021. E(n) equivariant graph neural networks. In *International conference on machine learning*, 9323–9332. PMLR.
- Song, Y.; Gong, J.; Xu, M.; Cao, Z.; Lan, Y.; Ermon, S.; Zhou, H.; and Ma, W.-Y. 2023a. Equivariant flow matching with hybrid probability transport for 3d molecule generation. *Advances in Neural Information Processing Systems*, 36: 549–568.
- Song, Y.; Gong, J.; Xu, M.; Cao, Z.; Lan, Y.; Ermon, S.; Zhou, H.; and Ma, W.-Y. 2023b. Equivariant flow matching with hybrid probability transport for 3d molecule generation. *Advances in Neural Information Processing Systems*, 36: 549–568.
- Song, Y.; Gong, J.; Zhou, H.; Zheng, M.; Liu, J.; and Ma, W.-Y. 2023c. Unified generative modeling of 3d molecules with bayesian flow networks. In *The Twelfth International Conference on Learning Representations*.
- Song, Y.; Sohl-Dickstein, J.; Kingma, D. P.; Kumar, A.; Ermon, S.; and Poole, B. 2021. Score-Based Generative Modeling through Stochastic Differential Equations. In *International Conference on Learning Representations*.
- Watson, J. L.; Juergens, D.; Bennett, N. R.; Trippe, B. L.; Yim, J.; Eisenach, H. E.; Ahern, W.; Borst, A. J.; Ragotte, R. J.; Milles, L. F.; et al. 2023. De novo design of protein structure and function with RFDiffusion. *Nature*, 620(7976): 1089–1100.
- Xu, M.; Powers, A. S.; Dror, R. O.; Ermon, S.; and Leskovec, J. 2023. Geometric latent diffusion models for 3d molecule generation. In *International Conference on Machine Learning*, 38592–38610. PMLR.
- Zhang, P.; Baker, D.; Song, M.; and Bi, J. 2025. Unraveling the potential of diffusion models in small-molecule generation. *Drug Discovery Today*, 104413.
- Zhang, Z.; Chen, Y.; and Chu, S. 2025. D3MES: Diffusion Transformer with multihead equivariant self-attention for 3D molecule generation. *arXiv preprint arXiv:2501.07077*.

A Experiment Details

This section describes the full experiment setup in this paper.

Hyperparameters All experiments are conducted on a single NVIDIA A100 40GB GPU. The search space for model and training hyperparameters are listed in Table 4. VEDA-S was trained using the data splits and adaptive data loader from Irwin et al. (2025).

Metrics To enable fair and consistent evaluation, we follow the metrics and baseline settings widely adopted in previous works on 3D molecular generation (e.g., EDM(Hoogeboom et al. 2022), SemlaFlow(Irwin et al. 2025)) and the benchmarks (Nikitin et al. 2025).

- **Atom Stability:** Percentage of atoms that satisfy standard valence rules.
- **Molecule Stability:** Percentage of molecules in which all atoms are stable.
- **Validity:** Percentage of molecules that can be parsed into valid SMILES strings via RDKit.
- **Validity & Uniqueness:** Fraction of unique samples within the set of valid molecules.
- **Conformational Energy (MMFF):** Estimated using the MMFF94 force field in RDKit; lower energy implies more realistic molecular structures.
- **Strain Energy (MMFF):** Energy difference between the initial and optimized conformations under MMFF; reflects post-processing effort for physical plausibility.
- **RMSD (xTB):** Root Mean Square Deviation between the initial and optimized conformations using the xTB toolkit.
- **RMSD (MMFF):** RMSD computed under MMFF force field.
- $\Delta E_{\text{relax}}(\text{xTB})$: Energy decrease after xTB geometry optimization.
- **Bond Length Deviation:** Mean absolute error (MAE) of bond lengths between initial and optimized structures:

$$\Delta r_{ij} = r_{ij}^{\text{init}} - r_{ij}^{\text{opt}}$$

- **Bond Angle Deviation:** MAE between initial and optimized bond angles:

$$\Delta \theta_{ijk} = \min \left(\left| \theta_{ijk}^{\text{init}} - \theta_{ijk}^{\text{opt}} \right|, 180^\circ - \left| \theta_{ijk}^{\text{init}} - \theta_{ijk}^{\text{opt}} \right| \right)$$

- **Torsion Angle Deviation:** MAE between initial and optimized torsion angles (a.k.a. dihedral angles):

$$\Delta \phi_{ijkl} = \min \left(\left| \phi_{ijkl}^{\text{init}} - \phi_{ijkl}^{\text{opt}} \right|, 360^\circ - \left| \phi_{ijkl}^{\text{init}} - \phi_{ijkl}^{\text{opt}} \right| \right)$$

Self-Conditioning Following the configuration of the SemlaFlow baseline (Irwin et al. 2025), we incorporate a self-conditioning mechanism for the VEDA-S model to enhance generation quality. This technique involves augmenting the model input with a preliminary estimate of the clean data, denoted as \tilde{x}_0 .

- **Training:** We employ a stochastic conditioning strategy. With a probability of 0.5, the model performs an initial forward pass to estimate \tilde{x}_0 , which is then concatenated with the noisy input for the final prediction. In the remaining 50% of cases, the conditioning input is set to zero (null condition).
- **Sampling:** Self-conditioning is active for all inference steps except the initial one (where no prior estimate exists). The estimate of the clean data derived from the previous timestep t_{i-1} is used as the condition for the current step t_i .

Note that this mechanism is exclusive to VEDA-S and is not employed in the VEDA-E architecture.

B Supplementary experiments

We also report results following the same metrics as SemlaFlow(Irwin et al. 2025), as shown in Table 5. Due to scalability limitations, UniGEM(Feng et al. 2024) and GeoBFN(Song et al. 2023c) are excluded. VEDA maintains high validity and significantly improves energy metrics in both bond-implicit and bond-explicit settings, reinforcing its robustness on large and chemically diverse molecules.

Sampling Efficiency and Speed of VEDA-E on QM9

We assess VEDA-E using two samplers—a first-order method and a second-order method—and compare against EDM (Hoogeboom et al. 2022) run with both the DDIM and the original DDPM samplers. Figure 5 presents the trade-off between sample quality and the number of function evaluations (NFE).

SemlaFlow on Different Noise Injection

We evaluate the performance of SemlaFlow under varying levels of noise injection. Specifically, at each noise level γ , the sampling step adds scaled Gaussian noise $\gamma\epsilon$, where $\epsilon \sim \mathcal{N}(0, 1)$. The results are summarized in Table 6, using the benchmark protocol from Nikitin et al. (2025). Although SemlaFlow (Irwin et al. 2025) reports $\gamma = 0.2$ in their paper, we find that their open-source implementation sets $\gamma = 0$. We therefore include a range of γ values in our experiments to assess its effect. Overall, SemlaFlow does not appear to benefit significantly from increased noise levels. Most metrics, including RMSD and energy relaxation, show marginal or inconsistent changes across different γ values, suggesting limited robustness or gain from additional noise injection.

Low-Confidence Re-masking Strategies

In iterative generative models, a key design choice is the strategy for selecting which tokens to mask and regenerate at each step. An intuitive heuristic, inspired by work like MaskGIT (Chang et al. 2022), is to focus on regions of low model confidence, with the goal of correcting the most

Hyperparameter	QM9		GEOM-DRUGS	
	VEDA-E	VEDA-S	VEDA-E	VEDA-S
Learning rate	3e-4	3e-4	1e-3	3e-4
Warm up steps	2000	15000	2000	10000
Batch Size	32	N/A	4	N/A
Batch Cost	N/A	4096	N/A	4096
EMA decay rate	0.9999	0.999	0.9999	0.999
T_{min}	0.001	0.001	0.001	0.001
T_{max}	80	80	80	80
σ_d	1	1	1	1
Training iterations	2000	300	10	200
Optimizer	Adam	Adam	Adam	Adam
EGNN layer	9	N/A	4	N/A
Features per layer	256	256	256	256
Activations Function	SiLU	SiLU	SiLU	SiLU
Semla n_{head}	N/A	32	N/A	32
Loss weight ($\lambda_x, \lambda_a, \lambda_b, \lambda_c$)	(1.0, 1.0, N/A, 1.0)	(1.0, 0.2, 0.5, 1.0)	(1.0, 1.0, N/A, 1.0)	(1.0, 0.2, 1.0, 1.0)
Noise scheduler ρ	2.5	2.5	2.5	2.5
categorical noise level η	N/A	1	N/A	1
Sampling Temperature (τ)	1.0	0.9	1.0	1.0
Max w_{cat} (Clip)	N/A	10	N/A	10
Prediction Mode	Constant	Constant	Constant	Adaptive
Cat. Loss Weighting	N/A	$1/m(t)$	N/A	$1/m(t)$

Table 4: Hyperparameters used for training VEDA-E and VEDA-S models

Methods	NFE	Atom Stab \uparrow	Mol Stab \uparrow	Valid \uparrow	Energy _{MMFF} \downarrow	Strain _{MMFF} \downarrow	RMSD _{MMFF} \downarrow
EDM	1000	81.3	N/A	92.6	-	-	-
GeoLDM	1000	84.4	N/A	99.6	-	-	-
UniGEM	1000	85.1	N/A	98.4	-	-	-
EquiFM	1000	84.1	N/A	98.9	-	-	-
GOAT	90	84.8	N/A	96.2	-	-	-
VEDA-E	50	88.7	3.6	97.3	-	-	-
VEDA-E	100	90.0	8.2	99.5	-	-	-
MiDi	500	99.8	91.6	77.8	-	-	-
EQGAT-diff*	500	99.8	93.4	94.6	68.8	28.9	1.115
SemlaFlow	100	99.8	97.7	95.2	127.5	88.9	0.857
FlowMol-CTMC*	250	99.9	95.7	90.1	71.1	37.5	1.255
VEDA-S	100	99.8	98.1	98.9	43.0	12.7	0.554
VEDA-S	50	99.5	93.3	95.3	61.2	20.7	0.714
Data	-	100	100	100	50.3	15.9	-

Table 5: Molecular generation results on the GEOM-DRUGS dataset. VEDA-S with Semla as the backbone. Molecule stability and validity are reported as percentages, while energy and strain energy are expressed in kcal-mol⁻¹. Results marked with * were reproduced in our own experiments. All results are calculated based on 1000 randomly sampled molecules.

Model	NFE	MS \uparrow	V&C \uparrow	Bond Length \downarrow ($\times 10^{-2}$)	Bond Angles \downarrow	Torsions \downarrow	Median ΔE_{relax} \downarrow	Mean ΔE_{relax} \downarrow	Median RMSD \downarrow	Mean RMSD \downarrow
SemlaFlow($\gamma=0$)	100	0.969	0.920	3.10	2.06	6.05	32.3	91.0	0.273	0.358
SemlaFlow($\gamma=0.01$)	100	0.969	0.928	2.90	1.92	5.47	31.7	72.6	0.252	0.368
SemlaFlow($\gamma=0.03$)	100	0.973	0.934	2.88	1.93	5.66	31.9	67.5	0.250	0.382
SemlaFlow($\gamma=0.1$)	100	0.978	0.933	2.87	1.92	5.56	31.6	67.0	0.269	0.383
SemlaFlow($\gamma=0.2$)	100	0.975	0.932	2.93	1.95	5.68	33.8	77.6	0.254	0.384
SemlaFlow($\gamma=0.4$)	100	0.970	0.926	2.88	1.93	5.61	31.6	71.0	0.256	0.387

Table 6: Performance comparison on the GEOM-DRUGS dataset using the benchmark from Nikitin et al. (2025). Noise is added according to $v = v + \epsilon \cdot \gamma$, where $\epsilon \sim \mathcal{N}(0, 1)$. Although SemlaFlow (Irwin et al. 2025) reports $\gamma = 0.2$ in their paper, their open-source implementation uses $\gamma = 0$.

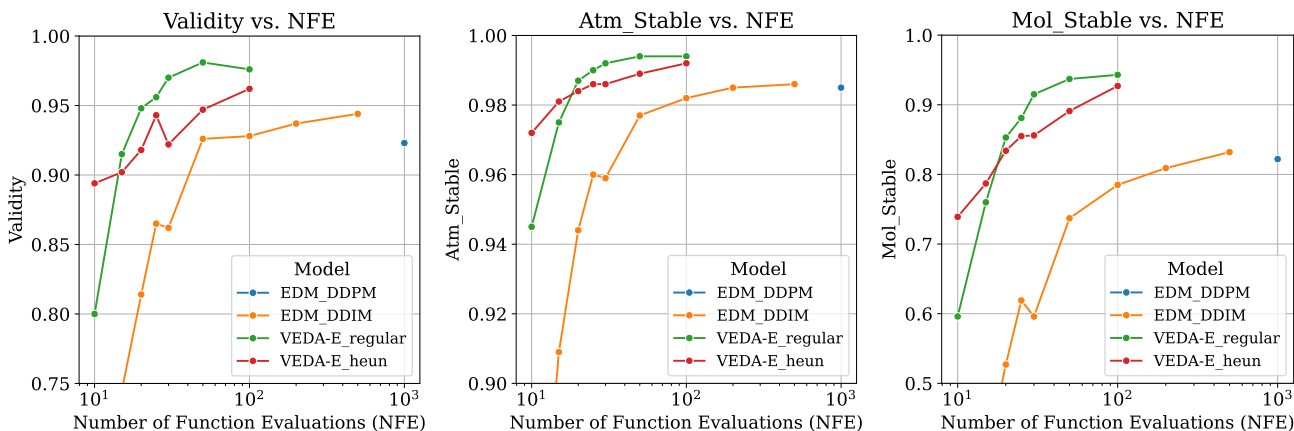


Figure 5: Quality–efficiency trade-off for VEDA-E on QM9 under different sampling strategies, compared with EDM (Hooeboom et al. 2022). Even at low NFE, our model sustains high validity and structural stability.

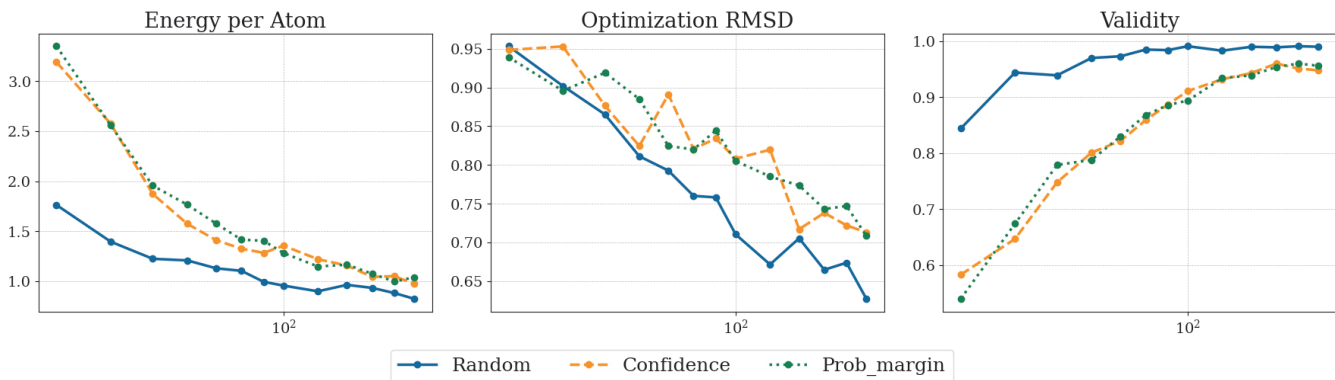


Figure 6: Comparison of re-masking strategies. The x-axis is the sampling steps. The performance of a Uniform Random strategy is compared against two confidence-based heuristics: selecting tokens with the lowest prediction confidence (*Confidence*) or the smallest probability margin (*Prob_margin*). The random strategy consistently achieves lower energy, lower optimization RMSD, and higher validity, indicating its superiority for this generative task.

likely errors. To investigate this, we explored two distinct confidence-based re-masking strategies:

Lowest Confidence: This strategy prioritizes re-masking tokens for which the model assigned the lowest probability to the predicted token. This directly targets the model’s points of highest uncertainty.

Smallest Probability Margin: This strategy selects tokens where the difference between the probabilities of the most likely and second-most likely predictions is minimal. This targets tokens where the model is highly ambivalent between multiple outcomes.

We compared these two heuristic approaches against a baseline **Uniform Random** strategy, which selects tokens for re-masking uniformly at random from all available positions.

The results of this comparison are presented in Figure 6, evaluated across three critical metrics: *Energy per Atom*, a measure of the thermodynamic stability of the generated molecule, where lower values indicate more physi-

cally plausible structures; *Optimization RMSD* (*Root Mean Square Deviation*), the geometric deviation between the as-generated structure and its energy-minimized (i.e., optimized) conformation, where lower values signify a better initial prediction; and *Validity*, the percentage of generated outputs that are chemically valid molecules.

As demonstrated in Figure 6, the Uniform Random strategy consistently and significantly outperforms both confidence-based methods across all three metrics. It converges to states with lower energy, produces geometries with lower RMSD to their optimized counterparts, and achieves a higher validity rate more quickly.

This finding suggests that, for this task, the stochasticity introduced by random selection is more beneficial for exploring the solution space and avoiding local minima than a greedy focus on correcting low-confidence predictions. While seemingly counter-intuitive, this indicates that the model’s confidence scores may not be the most reliable guide for iterative refinement.

C Ablation Studies

Ablation Study on various Discrete Sampling methods

The choice of the discrete sampling strategy and its associated hyperparameters is critical to the quality of the final generated structures. In Figure 7, we present a detailed comparison of the three sampler configurations discussed in the main text. The x-axis represents the hyperparameter η , which controls the categorical noise level, plotted on a symmetrical log scale to provide clarity for both small and large values. The y-axes correspond to three critical performance metrics: Energy per Atom (lower is better), Optimization RMSD (lower is better), and Validity (higher is better). Our analysis reveals that both the fixed and variable η_t schedules of Campbell et al. (2024)’DFM can both achieve top-tier performance, as long as on the appropriate selection of the noise hyperparameter η . For instance, the fixed η_t model (solid orange) reaches its optimal Validity near $\eta=0.3$. Similarly, the variable η_t model (dashed blue) finds its performance sweet spot in the region of η near 1.0. This indicates that the primary factor for success is tuning η correctly, rather than the choice between a fixed or variable schedule itself. While both can reach a similar performance minimum, the variable η_t schedule appears to offer a slightly wider range of near-optimal performance, potentially making it more robust. Conversely, the fixed η_t strategy is simpler and equally effective when η is precisely tuned. Based on this analysis, we conclude that the performance difference between the fixed and variable η_t schedules is not decisive. Given its slightly broader optimal range, we selected the Campbell et al. (2024)’DFM sampler with the variable η_t schedule for our main experiments, with η tuned to 1.0.

D Additional Implementation Details

This section elaborates on the hyperparameter configurations, stabilization mechanisms, and architectural variants used in our experiments.

Alternative Model Configurations To evaluate the robustness of our method, we provide comparisons between different residual prediction modes and mask rate schedules:

- **Residual Prediction Mode:** This configuration dictates how the input is subtracted from the network output to formulate the denoising target.
 - *Adaptive (Default):* Uses the optimal LMMSE coefficient derived in Appendix I. The network predicts a residual where the input is scaled by a time-dependent factor α_t :

$$\mathbf{x}_{\text{out}} = F_{\theta}(\mathbf{x}_{\text{in}}) - \alpha_t \mathbf{x}_{\text{in}}, \quad \text{where } \alpha_t = \frac{\sigma_d t}{\sigma_d^2 + t^2}.$$

- *Constant:* A simplified residual connection where the input is subtracted directly without scaling (effectively setting $\alpha_t = 1$). This forces the network to predict the pure residual $\mathbf{x}_{\text{out}} = F_{\theta}(\mathbf{x}_{\text{in}}) - \mathbf{x}_{\text{in}}$.

- **Mask Rate Schedule:** This determines the mapping from the continuous noise level t to the discrete mask rate $m(t) \in [0, 1]$.

- *Log-uniform (Default):* Linearly maps the logarithmic noise level $\ln(t)$ to the mask rate $m(t)$. This ensures that the discrete masking process is uniformly distributed with respect to the logarithmic time scale used by the continuous diffusion.
- *Sigmoid-style (EDM):* Adopts a sigmoid-like mapping derived from the ratio of noise to data weight, commonly used in discrete flow matching to map unbounded diffusion time $t \in [0, \infty)$ to a bounded probability:

$$m(t) = \frac{t}{t + \sigma_d}.$$

Training and Sampling Dynamics We incorporate two specific mechanisms to stabilize training and refine the generation process:

- **Categorical Loss Weighting:** While heuristic objectives like MaskGIT (Chang et al. 2022) have shown promise, they often lack the scaling terms required for a rigorous link to maximum likelihood estimation (Nie et al. 2025). To bridge this gap and balance the training objective, we employ a time-dependent weighting scheme inversely proportional to the mask rate:

$$w_{\text{cat}}(t) = \min\left(\frac{1}{m(t)}, 10\right).$$

By incorporating this $1/m(t)$ factor, we ensure that time steps with fewer masked tokens (low $m(t)$) are not under-represented in the total loss. The clipping mechanism further prevents numerical instability near $t = 0$, effectively combining theoretical motivation with training stability.

- **Sampling Temperature:** During the generation phase, we utilize a temperature parameter τ to rescale the logits of the categorical distributions (atom types, charges, and bond types) prior to the Softmax operation: $P(z_i) = \text{Softmax}(l_i/\tau)$, where l_i are the predicted logits. This parameter controls the stochasticity of the discrete transitions, balancing diversity with structural validity.

E Molecule Algorithm

This section details the sampling algorithms used for generating 3D molecules. We employ two distinct samplers: a standard diffusion stochastic sampler for models handling only continuous coordinates (Algorithm 1), and an extended masked diffusion sampler for our primary model that jointly generates continuous coordinates and discrete atomic features (Algorithm 2).

Algorithm 1 outlines the standard stochastic sampler for a diffusion model operating on continuous variables, such as atomic coordinates \mathcal{M} . The process begins by sampling an initial state from a Gaussian distribution at the maximum noise level t_0 (Line 2). The core of the algorithm is an iterative loop that progressively denoises the sample. In each

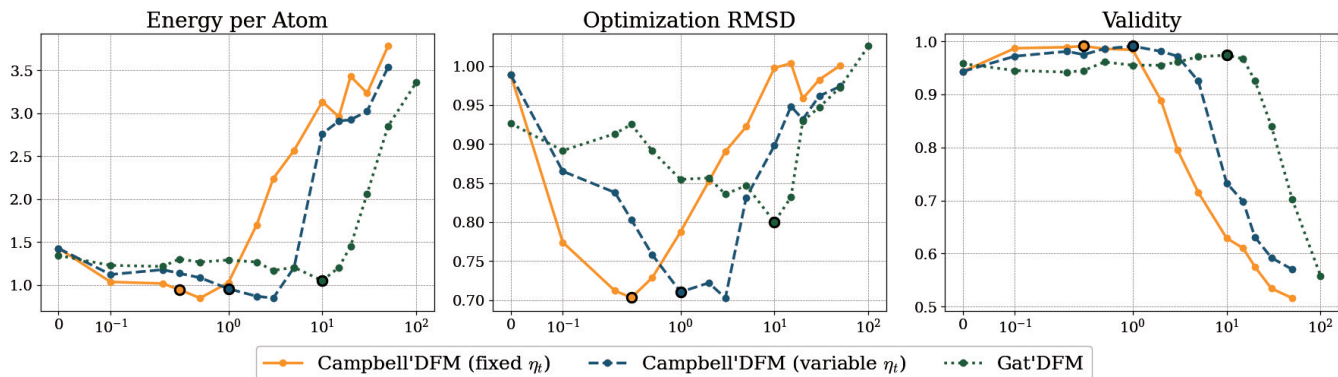


Figure 7: Hyperparameter tuning for DFM sampling strategies. We compare the performance of two distinct sampling approaches derived from the Discrete Flow Matching (DFM) framework. The first approach, based on the transition rate formulation of Campbell et al. (2024), is evaluated with both a fixed η_t (solid orange line) and a variable η_t schedule (dashed blue line). The second approach is the simplified velocity-field method from Gat et al. (2024), denoted as Gat'DFM (dotted green line). Performance is measured across three metrics—Energy per Atom, Optimization RMSD, and Validity—as a function of the categorical noise level hyperparameter η . The results show that the variable η_t schedule provides the most robust trade-off, significantly minimizing optimization RMSD while maintaining high structural validity across a wide range of noise levels.

step, a small amount of noise is first added to the current sample \mathcal{M}_i to create a perturbed state $\hat{\mathcal{M}}_i$ (Lines 5-6). This stochastic step (often called "churn") helps in error correction and exploration. The model f_θ then predicts the denoised version of $\hat{\mathcal{M}}_i$, from which a denoising direction d_i is computed (Line 7). Finally, the sample is updated by taking a step in this direction to arrive at the less noisy state \mathcal{M}_{i+1} (Line 8). This process is repeated until the noise level reaches zero, yielding the final molecular structure.

Algorithm 2 extends this framework to a multi-modal scenario, jointly generating continuous coordinates (\mathbf{x}) and discrete atomic types (\mathbf{z}). The process similarly starts from pure noise for both modalities (Line 2), with atom types initialized from a uniform categorical distribution. The key distinction lies in the iterative update loop. Both coordinates and atom types are corrupted with modality-specific noise (Lines 6-7); coordinates receive Gaussian noise, while atom types are randomly masked by mixing with a uniform distribution. The model f_θ takes this combined noisy input and jointly predicts the clean coordinates and atom types (Line 8). While the coordinate update follows the same procedure as in Algorithm 1 (Lines 9-10), the discrete atom types are updated using a specialized `DiscreteSampler` (Line 11). This sampler is designed to handle categorical variables and implements a discrete flow matching (DFM) process, ensuring that the updates for atomic types are valid and effective. The final output is a complete 3D molecule with both its geometry and chemical composition specified.

F Experiments of various sampling steps

As shown in Table 7, our VEDA-S model consistently achieves state-of-the-art performance across most metrics, even at a low number of sampling steps (e.g., 100), outperforming prior methods like SemlaFlow and FlowMol2 in terms of molecule stability and RMSD.

Algorithm 1: Diffusion Stochastic Sampler

```

1: Input: Sampling steps  $t_0 > \dots > t_N = 0$ , model  $f_\theta(\mathcal{M}, t)$ , noise scale  $S_{\text{noise}}$ 
2: Sample  $\mathcal{M} \sim \mathcal{N}(0, t_0^2 I)$ 
3: for  $i = 0$  to  $N - 1$  do
4:   Sample  $\epsilon_i \sim \mathcal{N}(0, I)$ 
5:    $\hat{t}_i \leftarrow t_i + \gamma_i t_i$ 
6:    $\hat{\mathcal{M}}_i \leftarrow \mathcal{M}_i + \sqrt{\hat{t}_i^2 - t_i^2} \cdot \epsilon_i$ 
   {▷ Increased noise level from  $t_i$  to  $\hat{t}_i$ }
7:    $d_i \leftarrow (\hat{\mathcal{M}}_i - f_\theta(\hat{\mathcal{M}}_i, \hat{t}_i)) / \hat{t}_i$ 
8:    $\mathcal{M}_{i+1} \leftarrow \hat{\mathcal{M}}_i + (t_{i+1} - \hat{t}_i) \cdot d_i$ 
9: end for
10: Output:  $x_N$ 

```

G Derivation of Transition Rates Matrix for the Masking Process

Following the derivation of Discrete Flow Matching (Campbell et al. 2024), we will derive the form R^* , representing the transition rate from the current state x_t to each state j , with respect to t and x_0 . Let the number of categories be S , and the mask rate function satisfy $m(t) \in [0, 1]$ with $m'(t) > 0$. Denote by

$$\delta(i, x_0) = \begin{cases} 1, & i = x_0, \\ 0, & i \neq x_0, \end{cases}$$

the Kronecker delta. We interpolate between the point mass at x_0 and the uniform distribution:

$$p(x_t) = \text{Cat}((1 - m(t))\delta(x_t, x_0) + \frac{m(t)}{S}). \quad (17)$$

Predictive Term Define the instantaneous transition rate from state x_t to state j as

$$R^*(x_t, j) = \frac{\text{ReLU}(\partial p(j) - \partial p(x_t))}{S p(x_t)}. \quad (18)$$

Model	NFE	MS \uparrow	V&C \uparrow	Bond Length \downarrow ($\times 10^{-2}$)	Bond Angles \downarrow	Torsions \downarrow	Median ΔE_{relax} \downarrow	Mean ΔE_{relax} \downarrow	Median RMSD \downarrow	Mean RMSD \downarrow
EQGAT	250	0.318	0.605	2.63	3.01	17.63	34.95	76.49	0.974	1.044
EQGAT	500	0.899	0.834	1.00	1.15	8.58	6.40	11.1	0.915	0.975
JODO	500	0.963	0.879	0.77	0.83	6.01	4.74	7.04	-	-
Megalodon-quick	500	0.944	0.900	0.66	0.71	5.58	3.19	5.76	-	-
FlowMol2	50	0.750	0.694	1.87	1.99	16.22	23.9	31.34	0.947	1.024
FlowMol2	100	0.830	0.768	1.54	1.78	15.45	21.0	27.1	0.992	1.038
FlowMol2	150	0.883	0.796	1.37	1.65	14.90	20.1	25.8	0.950	1.011
FlowMol2	200	0.902	0.803	1.26	1.61	14.70	16.9	23.5	0.981	0.999
FlowMol2	250	0.892	0.807	1.30	1.60	14.59	17.8	23.9	0.954	1.007
SemlaFlow	50	0.965	0.899	2.97	2.02	6.52	33.2	93.6	0.310	0.433
SemlaFlow	100	0.969	0.920	3.10	2.06	6.05	32.3	91.0	0.273	0.358
SemlaFlow	150	0.971	0.943	2.88	1.92	5.11	31.5	68.7	0.230	0.349
SemlaFlow	200	0.974	0.942	2.86	1.90	4.93	31.4	90.4	0.227	0.355
SemlaFlow	250	0.978	0.933	2.84	1.87	4.86	30.4	95.0	0.216	0.338
Megalodon-flow	100	0.987	0.948	2.30	1.62	5.58	20.9	46.9	-	-
VEDA-S	50	0.968	0.966	0.86	0.60	5.10	2.99	8.38	0.236	0.355
VEDA-S	75	± 0.001	± 0.010	± 0.02	± 0.04	± 0.39	± 0.34	± 2.05	± 0.055	± 0.042
VEDA-S	100	0.992	0.981	0.73	0.46	3.38	2.06	6.66	0.138	0.262
VEDA-S	100	0.995	0.988	0.69	0.41	2.71	1.72	2.93	0.096	0.197
VEDA-S	125	± 0.001	± 0.003	± 0.02	± 0.02	± 0.25	± 0.17	± 0.13	± 0.02	± 0.03
VEDA-S	150	0.999	0.986	0.69	0.38	2.24	1.61	2.55	0.084	0.161
VEDA-S	200	0.995	0.991	0.66	0.36	1.94	1.43	2.16	0.073	0.131
VEDA-S	250	0.999	0.993	0.65	0.34	1.68	1.35	1.99	0.064	0.114
VEDA-S	250	0.998	0.987	0.67	0.34	1.59	1.34	2.06	0.061	0.107

Table 7: Performance comparison on the GEOM-DRUGS dataset following the benchmark of Nikitin et al. (2025). Results for FlowMol2, EQGAT, SemlaFlow, and VEDA-S are reported under different sampling steps. VEDA-S is evaluated using 5000 generated samples at 50 and 100 steps, with standard deviations computed over 5 subsets. All other methods are evaluated on 1,000 generated samples.

Algorithm 2: Masked Diffusion Stochastic Sampler for Joint Coordinate and Atom-Type Generation

```

1: Input: Sampling steps  $t_0 > \dots > t_N = 0$ , model  $f_\theta(\{\mathbf{x}, \mathbf{z}\}, t)$ , mask_rate function  $m(t)$ , number of category  $S$ 
2: Sample  $\mathbf{x}_0 \sim \mathcal{N}(0, t_0^2 I)$ ,  $\mathbf{z}_0 \sim \text{Cat}(\frac{1}{S}, \dots, \frac{1}{S})$ 
3: for  $i = 0$  to  $N - 1$  do
4:   Sample  $\epsilon_i \sim \mathcal{N}(0, I)$ 
5:    $\hat{t}_i \leftarrow t_i + \gamma_i t_i$ 
6:    $\hat{\mathbf{x}}_i \leftarrow \mathbf{x}_i + \sqrt{\hat{t}_i^2 - t_i^2} \cdot \epsilon_i$ 
7:    $\hat{\mathbf{z}}_i \sim \text{Cat}[(1 - r_i) \cdot \delta_{\mathbf{z}_i} + r_i \cdot \text{Unif}(1, S)]$ 
8:    $\mathbf{x}_{\text{pred}}, \mathbf{z}_{\text{pred}} \leftarrow f_\theta(\{\hat{\mathbf{x}}_i, \hat{\mathbf{z}}_i\}, \hat{t}_i)$ 
9:    $\mathbf{d}_i \leftarrow (\hat{\mathbf{x}}_i - \mathbf{x}_{\text{pred}}) / \hat{t}_i$ 
10:   $\mathbf{x}_{i+1} \leftarrow \hat{\mathbf{x}}_i + (t_{i+1} - \hat{t}_i) \cdot \mathbf{d}_i$ 
11:   $\mathbf{z}_{i+1} \leftarrow \text{Discrete\_Sampler}(\hat{\mathbf{z}}_i, \mathbf{z}_{\text{pred}}, m(\hat{t}_i) - m(t_{i+1}))$ 
12: end for
13: Output:  $(\mathbf{x}_N, \mathbf{z}_N)$ 

```

Since

$$\partial p(x_t) = \partial((1 - m(t)) \delta(x_t, x_0) + \frac{m(t)}{S}) \quad (19)$$

$$= -m'(t) \delta(x_t, x_0) + \frac{m'(t)}{S} \quad (20)$$

we obtain

$$R^*(x_t, j) = -\frac{\text{ReLU}(\delta(j, x_0) - \delta(x_t, x_0)) m'(t)}{S((1 - m(t)) \delta(x_t, x_0) + \frac{m(t)}{S})} \quad (21)$$

Noting that $R^*(x_t, j) \neq 0$ if and only if $x_t = j \neq x_0$, we simplify:

$$R^*(x_t, j) = \frac{m'(t)}{m(t)} \delta(j, x_0) (1 - \delta(x_t, x_0)) \quad (22)$$

$$(23)$$

Detailed Balanced Term The concept of detailed balance has been utilized in previous continuous-time Markov chain (CTMC) generative models, such as in the work by Campbell et al. (2024), to make adjustments for inference. We add a detailed-balance correction satisfying

$$p(i) R^{\text{DB}}(i, j) = p(j) R^{\text{DB}}(j, i), \quad (24)$$

We need to make some assumptions about the form of R^{DB} . When considering masking noise, a process that is in detailed balance will have a certain rate for transitions from a masked state to z_0 , as well as a certain rate for transitions from z_0 back to the masked state in order to cancel out this effect. The rate for such transitions would take the following form. So We have parameterized R^{DB} with two time-dependent pre-defined constants a_t and b_t . Therefore, when i and j are both not equal to z_0 , this term is zero, essentially

representing the diffusion flow between z_0 and other states and its reverse action.

$$R^{\text{DB}}(i, j) = a_t \delta(i, z_0) + b_t \delta(j, z_0). \quad (25)$$

$$p(i) = (1 - m(t)) \delta(i, z_0) + \frac{m(t)}{S} \quad (26)$$

This yields

$$((1 - m) \delta(i, z_0) + \frac{m}{S})(a_t \delta(i, z_0) + b_t \delta(j, x_0)) \quad (27)$$

$$= ((1 - m) \delta(j, z_0) + \frac{m}{S})(a_t \delta(j, z_0) + b_t \delta(i, z_0)). \quad (28)$$

For the case $x_0 = i$, $\delta(i, z_0) = 1$ and $\delta(j, z_0) = 0$, we have:

$$(1 - m(t) + \frac{m(t)}{S}) a_t = \frac{m(t)}{S} b_t \quad (29)$$

$$b_t = \frac{S - S m(t) + m(t)}{m(t)} a_t. \quad (30)$$

Introducing a noise strength parameter η , we set

$$R^{\text{DB}}(i, j) = \eta \delta(i, z_0) + \eta \frac{S - S m(t) + m(t)}{m(t)} \delta(j, x_0). \quad (31)$$

Full Transition Rate The full transition rate R^θ consists of two components: the base transition R^* , which arises from the interpolation between a point mass at the original category and a uniform distribution, and the correction term R^{DB} , which enforces detailed balance to ensure proper Markovian dynamics. The total rate is given by:

$$R^\theta(z_t, j) = \mathbb{E}_{p_{0|t}^\theta(z_0|z_t)} [R^*(z_t, j) + R^{\text{DB}}(z_t, j)] \quad (32)$$

$$= \mathbb{E}_{p_{0|t}^\theta(z_0|z_t)} \left[\frac{m'(t)}{m(t)} \delta(j, z_0) (1 - \delta(z_t, z_0)) + \eta \delta(z_t, z_0) + \eta \frac{S - S m(t) + m(t)}{m(t)} \delta(j, z_0) \right] \quad (33)$$

$$= \frac{\eta S (1 - m(t)) + \eta m(t) + m'(t)}{m(t)} p_{0|t}^\theta(z_0 = j | z_t) + \eta p_{0|t}^\theta(z_0 = z_t | z_t) \quad (34)$$

In this formulation, the term $p_{0|t}^\theta(z_0 = j | z_t)$ represents the predicted probability that the clean data corresponds to category j , and thus determines the transition rate from the current state z_t to j . The second term, $p_{0|t}^\theta(z_0 = z_t | z_t)$, represents the probability that the current noisy state z_t already matches the clean data, and therefore governs the rate of remaining in the current state.

Transition Rate under Our Mask Rate Schedule With our specific mask rate schedule

$$m(t) = \frac{\log(t/T_{\min})}{\log(T_{\max}/T_{\min})},$$

we can derive the explicit form of the transition rate. Taking the derivative with respect to time, we obtain

$$m'(t) = \frac{1}{t \log(T_{\max}/T_{\min})}.$$

$$R = \left[\eta S \frac{\log(T_{\max}/T_{\min})}{\log(t/T_{\min})} + \eta(1 - S) + \frac{1}{t \log(t/T_{\min})} \right] \quad (35)$$

$$p_{0|t}^\theta(x_0 = j | x_t) + \eta p_{0|t}^\theta(x_0 = x_t | x_t) \quad (36)$$

In our formulation, we replace the original time variable t in the base paper with a monotonic schedule function of mask rate $m(t)$. To match the effective categorical noise strength used in the original Discrete Flow Matching formulation (where t directly corresponds to the interpolation coefficient), one could compensate by dividing the noise parameter η by $m'(t)$. However, since the detailed balance condition holds for any constant scaling of η , this modification is not strictly required. In practice, we treat the inclusion or exclusion of the extra $m'(t)$ factor as a tunable hyperparameter, and adopt the version that includes it in our final implementation.

H Derivation of Transition Rates Matrix for the Masking Process

We also include the transition rate matrix formulation from Discrete Flow Matching (DFM) (Gat et al. 2024), which provides an alternative approach to modeling discrete diffusion dynamics. This approach offers computational efficiency through streamlined probability updates, making it particularly suitable for large-scale discrete token generation. The DFM approach constructs a velocity field using forward and backward components:

$$\bar{u}_t = \alpha_t \hat{u}_t - \beta_t \tilde{u}_t \quad (37)$$

where $\hat{u}_t = \frac{m'(t)}{m(t)}(p_\theta - p_{\text{curr}})$ represents the forward velocity toward model predictions, $\tilde{u}_t = \frac{m'(t)}{1-m(t)}(p_{\text{curr}} - p_{\text{noise}})$ represents the backward velocity, and α_t and β_t are time-dependent coefficients satisfying $\alpha_t + \beta_t = 1$. More specifically, $\alpha_t \propto \eta$, where η is the categorical noise level. The discrete transition probabilities are then updated as:

$$p_{\text{next}} = p_{\text{curr}} + \Delta m(t) \cdot \bar{u}_t \quad (38)$$

DFM Formulation Rather than directly computing transition rates, DFM constructs a velocity field using a mask rate schedule $m(t)$. The approach decomposes the dynamics into two velocity components:

- **Forward velocity:** $\hat{u}_t = \frac{m'(t)}{1-m(t)}(p_\theta - p_{\text{curr}})$, which drives transitions from the current state toward the model's predicted distribution
- **Backward velocity:** $\tilde{u}_t = \frac{m'(t)}{m(t)}(p_{\text{curr}} - p_{\text{noise}})$, which accounts for the reverse flow from the current state toward the noise distribution

Velocity Field Combination The final velocity field is constructed as a weighted combination:

$$\bar{u}_t = \alpha_t \hat{u}_t - \beta_t \tilde{u}_t$$

where the weighting parameters satisfy $\alpha_t + \beta_t = 1$ and are typically parameterized as: $\alpha_t = \eta(1 - m(t))^a m(t)^b$

with η , a , and b being hyperparameter that control the relative importance of forward and backward flows throughout the process.

Transition Rate Matrix The discrete transition probabilities are updated using: $p_{\text{next}} = p_{\text{curr}} + \Delta m(t) \cdot \bar{u}_t$

This formulation provides a direct way to compute transition rates by combining model predictions with the current state distribution, weighted by the time-dependent schedule $m(t)$ and its derivative $m'(t)$.

Comparison with Standard Diffusion Unlike our direct derivation of $R^*(x_t, j)$ from the interpolation dynamics, DFM’s approach allows for more flexible control over the masking dynamics through the choice of $m(t)$ and the hyperparameters governing α_t . Notably, DFM’s formulation is conceptually simpler than the (Campbell et al. 2024) framework, as it avoids special treatment of diagonal elements (i.e., no-transition cases) in the transition matrix. While DFM introduces some empirically-motivated hyperparameters, this simplicity provides better interpretability for downstream applications and facilitates debugging during implementation. The explicit separation into forward and backward components also provides clear intuition about the direction of information flow at each time step.

Although the backward velocity field in DFM serves to balance model predictions and can provide effects to avoid overly greedy sampling, our experiments reveal that it cannot fully substitute for explicit remasking and noise injection strategies, likely due to the multi-modal nature of molecular structures. Both methods enable iterative refinement of masked regions and improve the consistency and quality of generated discrete sequences.

I Derivation of Optimal α_t

In the main text, we propose to decouple the network’s learning task by isolating and subtracting the undesired linear component that arises from the network’s inductive bias toward identity-like functions. We formalize this by finding a coefficient α_t that provides the best linear estimate of the target noise $\sigma_d \epsilon$ given the noisy input \mathbf{x}_t .

This coefficient is the solution to the following Linear Minimum Mean Squared Error (LMMSE) problem:

$$\alpha_t = \arg \min_{\alpha} \mathbb{E}[\|\sigma_d \epsilon - \alpha \mathbf{x}_t\|^2] \quad (39)$$

The LMMSE framework is chosen because it provides a principled and optimal solution for this specific goal. Its use rests on two key premises. First, we deliberately constrain

the estimator to be **linear** (i.e., of the form $\alpha \mathbf{x}_t$), which directly corresponds to our objective of quantifying and removing the network’s linear bias. Second, we assume the **second-order statistics** (i.e., variances and covariances) of the random variables \mathbf{x}_t and ϵ are known. This assumption holds true in diffusion models, where these statistics are well-defined functions of the noise level t and data properties. The LMMSE formulation in Eq. (39) is the standard method for finding this optimal linear estimator.

To find the minimum, we differentiate the objective function $J(\alpha) = \mathbb{E}[\|\sigma_d \epsilon - \alpha \mathbf{x}_t\|^2]$ with respect to α and set the result to zero:

$$\frac{\partial J(\alpha)}{\partial \alpha} = \frac{\partial}{\partial \alpha} \mathbb{E}[(\sigma_d \epsilon)^T (\sigma_d \epsilon) - 2\alpha (\sigma_d \epsilon)^T \mathbf{x}_t + \alpha^2 \mathbf{x}_t^T \mathbf{x}_t] \quad (40)$$

$$= \mathbb{E}[-2(\sigma_d \epsilon)^T \mathbf{x}_t + 2\alpha \mathbf{x}_t^T \mathbf{x}_t] = 0 \quad (41)$$

Solving for α yields:

$$\alpha_t = \frac{\mathbb{E}[(\sigma_d \epsilon)^T \mathbf{x}_t]}{\mathbb{E}[\mathbf{x}_t^T \mathbf{x}_t]} = \frac{\text{Cov}(\sigma_d \epsilon, \mathbf{x}_t)}{\text{Var}(\mathbf{x}_t)} \quad (42)$$

where the second equality holds for zero-mean variables.

Following the standard diffusion model setup, the noisy sample is defined as $\mathbf{x}_t = \mathbf{x}_0 + t\epsilon$, where the clean data \mathbf{x}_0 and the standard Gaussian noise $\epsilon \sim \mathcal{N}(0, \mathbf{I})$ are independent. We adopt the setup from Karras et al. (2022), where $\text{Var}(\mathbf{x}_0) = \sigma_d^2$ and $\text{Var}(\epsilon) = 1$.

Covariance (Numerator):

$$\begin{aligned} \text{Cov}(\sigma_d \epsilon, \mathbf{x}_t) &= \text{Cov}(\sigma_d \epsilon, \mathbf{x}_0 + t\epsilon) \\ &= \sigma_d \text{Cov}(\epsilon, \mathbf{x}_0) + \sigma_d t \text{Var}(\epsilon) \\ &= 0 + \sigma_d t \cdot 1 = \sigma_d t \end{aligned}$$

Variance (Denominator):

$$\begin{aligned} \text{Var}(\mathbf{x}_t) &= \text{Var}(\mathbf{x}_0 + t\epsilon) \\ &= \text{Var}(\mathbf{x}_0) + t^2 \text{Var}(\epsilon) \\ &= \sigma_d^2 + t^2 \end{aligned}$$

Substituting these results gives the final expression:

$$\alpha_t = \frac{\sigma_d t}{\sigma_d^2 + t^2} \quad (43)$$

This choice of α_t removes the optimal linear estimate of the noise from the network’s output, thereby allowing the network to focus on learning the non-linear residual component.

J Derivation for the Smoothed Potential Energy Equivalence

Below, we provide a formal derivation for the claim made in the main text that adding Gaussian noise to coordinates is equivalent in expectation to sampling from a smoothed potential energy surface. We demonstrate this for the 3D case, which is relevant to molecular structures.

Let the molecular coordinates be $\mathbf{x} \in \mathbb{R}^3$ and the potential energy surface (PES) be the function $E(\mathbf{x})$.

First, let's define the smoothed PES, $\tilde{E}(\mathbf{x})$, as the convolution of the original surface $E(\mathbf{x})$ with a 3D Gaussian kernel $G(\mathbf{z}; \sigma^2)$:

$$\tilde{E}(\mathbf{x}) = \int_{\mathbb{R}^3} E(\mathbf{y}) G(\mathbf{x} - \mathbf{y}; \sigma^2) d\mathbf{y} \quad (44)$$

where $G(\mathbf{z}; \sigma^2)$ is the standard zero-mean Gaussian probability density function with variance σ^2 along each axis.

Our procedure involves adding Gaussian noise $\epsilon \sim \mathcal{N}(\mathbf{0}, \sigma^2 I)$ to the coordinates, resulting in a perturbed state $\mathbf{x}' = \mathbf{x} + \epsilon$. Our goal is to show that the expected energy of this new state is exactly the value of the smoothed potential at the original location \mathbf{x} , which can be expressed by:

$$\mathbb{E}_{\epsilon}[E(\mathbf{x} + \epsilon)] = \tilde{E}(\mathbf{x}) \quad (45)$$

We start from the definition of the expectation:

$$\begin{aligned} \mathbb{E}_{\epsilon}[E(\mathbf{x} + \epsilon)] &= \int_{\mathbb{R}^3} E(\mathbf{x} + \epsilon) p(\epsilon) d\epsilon \\ &= \int_{\mathbb{R}^3} E(\mathbf{x} + \epsilon) G(\epsilon; \sigma^2) d\epsilon \end{aligned}$$

Here, $p(\epsilon)$ is the probability density function of the noise, which is the Gaussian kernel G .

Next, we perform a simple change of variables by setting $\mathbf{y} = \mathbf{x} + \epsilon$. This implies $\epsilon = \mathbf{y} - \mathbf{x}$. Substituting this back into the integral gives:

$$\mathbb{E}_{\epsilon}[E(\mathbf{x} + \epsilon)] = \int_{\mathbb{R}^3} E(\mathbf{y}) G(\mathbf{y} - \mathbf{x}; \sigma^2) d\mathbf{y} \quad (46)$$

Recognizing that the Gaussian kernel is symmetric, i.e., $G(\mathbf{y} - \mathbf{x}) = G(\mathbf{x} - \mathbf{y})$, the right-hand side of the equation becomes identical to the definition of the smoothed potential $\tilde{E}(\mathbf{x})$ in Equation 44.

Thus, we have shown that:

$$\mathbb{E}_{\epsilon}[E(\mathbf{x} + \epsilon)] = \tilde{E}(\mathbf{x}) \quad (47)$$

This confirms that, on average, the energy of the noise-perturbed samples corresponds to the energy of a smoothed landscape, which facilitates exploration and helps the sampler avoid minor local minima.